Supplement of Atmos. Meas. Tech., 9, 553–576, 2016
http://www.atmos-meas-tech.net/9/553/2016/
doi:10.5194/amt-9-553-2016-supplement
© Author(s) 2016. CC Attribution 3.0 License.

Atmospheric Measurement Techniques
Open Access

Supplement of

A two-channel thermal dissociation cavity ring-down spectrometer for the detection of ambient NO_2, RO_2NO_2 and $RONO_2$

J. Thieser et al.

Correspondence to: J. N. Crowley (john.crowley@mpic.de)

The copyright of individual parts of the supplement might differ from the CC-BY 3.0 licence.

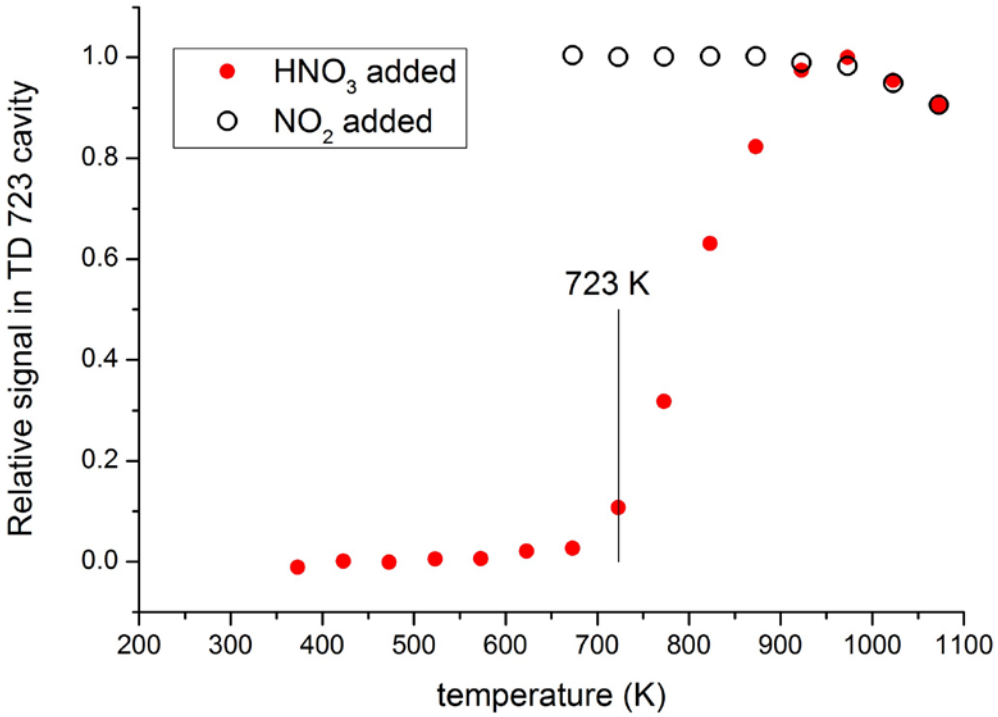

Figure S1 Efficiency of detection of HNO_3 as NO_2 in the TD inlet at 723 K. The red datapoints were obtained by flowing a few ppbv of HNO_3 from a permeation source to the instrument. The amount of NO_2 detected at 723 K is ~ 10 % of that observed at ~950 K, where HNO_3 is expected to be quantitatively converted to NO_2. The decrease in NO_2 signal at T > 950 K is due to NO_2 thermal decomposition on the quartz surfaces (open, black circles).

1

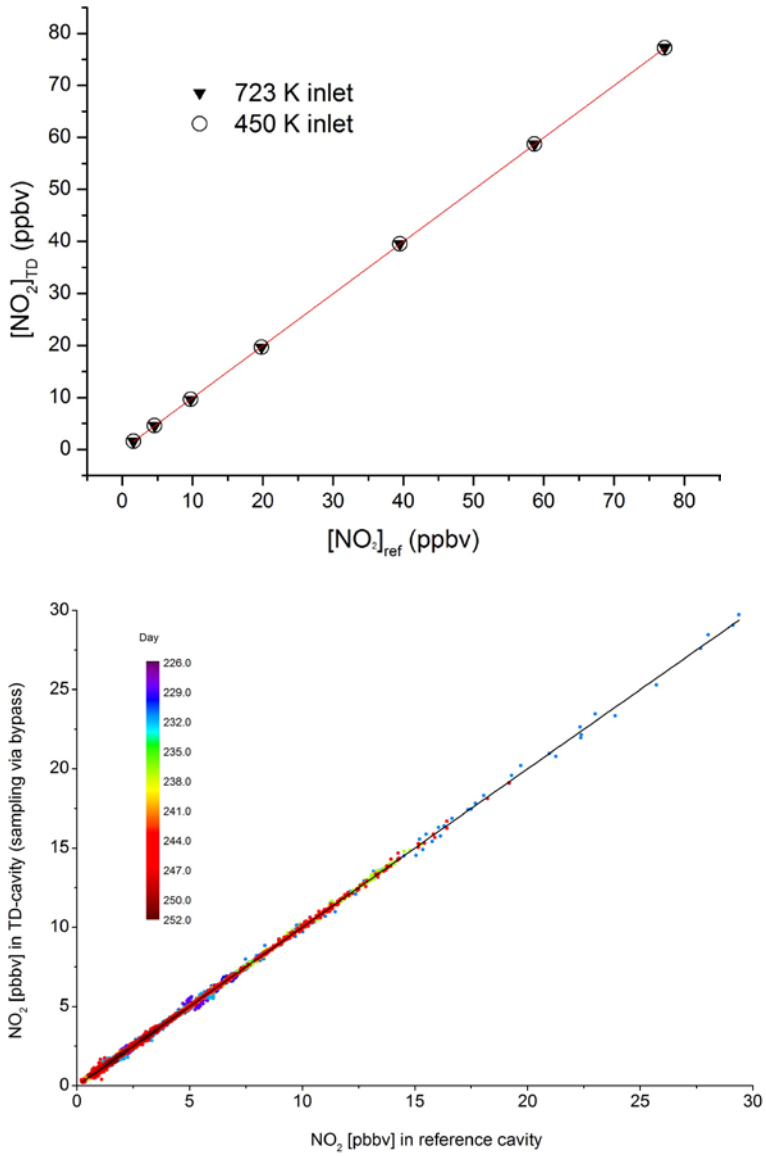

Figure S2 Upper panel: Comparison of response of the TD-cavity to additions of NO_2. The reference cavity samples from the inlet at ambient temperature, the TD-cavity from inlets at either 473 or 723 K. The slope of the regression line is 1.000 ± 0.001 in both cases. Lower panel: Comparison of NO_2 mixing ratios obtained during the PARADE campaign using the reference cavity with those obtained when sampling via the non-heated bypass into the TD-cavity. The slope is 0.9997 ± 0.0002. The colour code indicates that these measurements were taken over a period of 26 days, and the data covers ~ 10 % of the entire instrument operation time.

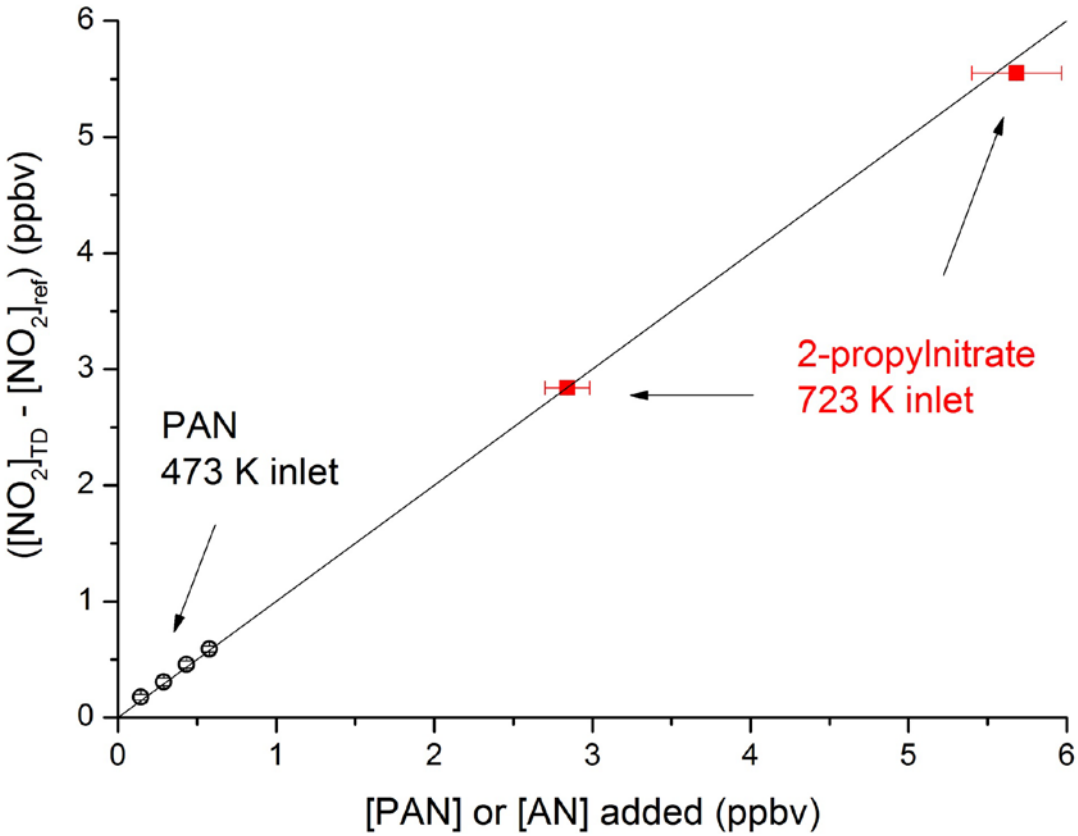

Figure S3. Addition (not simultaneous) of known amounts of PAN (black data points) and 2-propylnitrate to the 473 K and 723 K inlets, respectively. The solid line represents the 1:1 conversion of both PAN and 2-propylnitrate to NO_2.

1

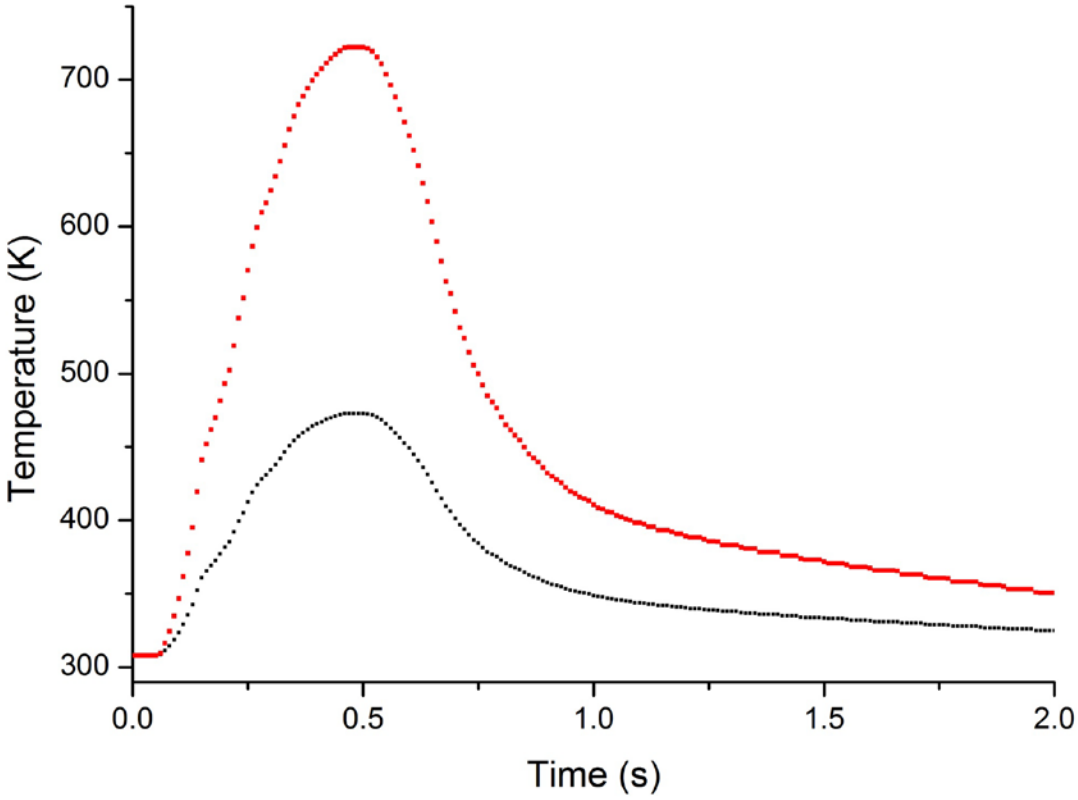

Figure S4. Temperature profiles used in simulations. Time = 0 is when the gas passes the front edge of the oven. Red curve = 723 K oven, black curve = 473 K oven.

1

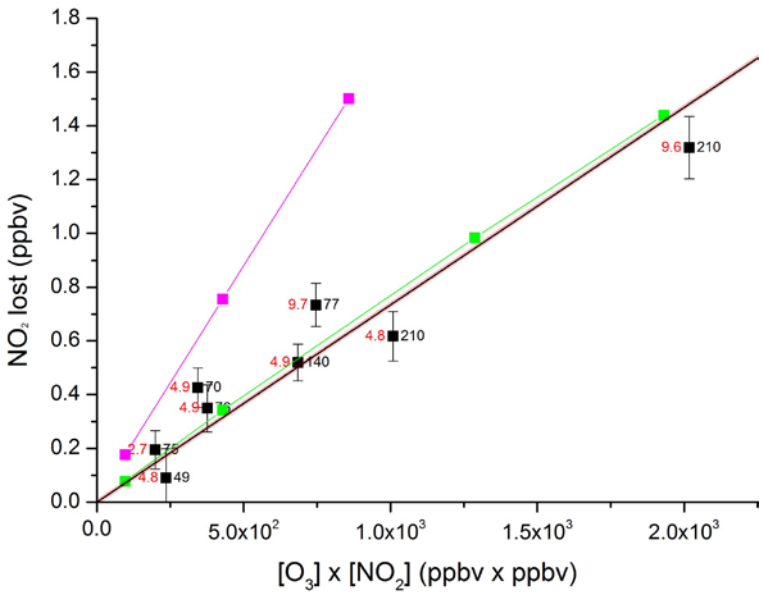

Figure S5. *Upper panel:* The same as Figure 6b in the main manuscript but with numerical simulations of the effect of thermal dissociation of O_3 with (green symbols) and without (purple symbols) O-atom wall losses.

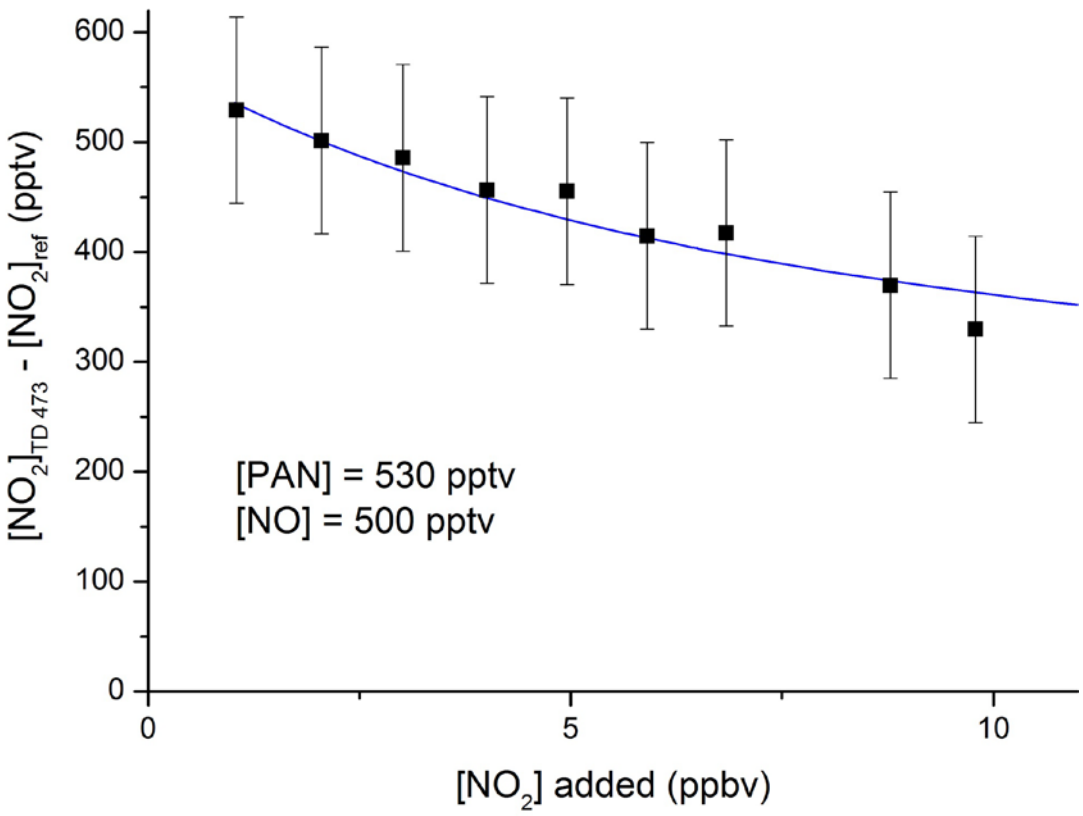

Figure S6. NO_2 formed in the TD channel at 473 K from adding various amounts of NO_2 (up to 10 ppbv) to 560 pptv PAN in presence of NO (500 pptv). The blue line is the model prediction.

1

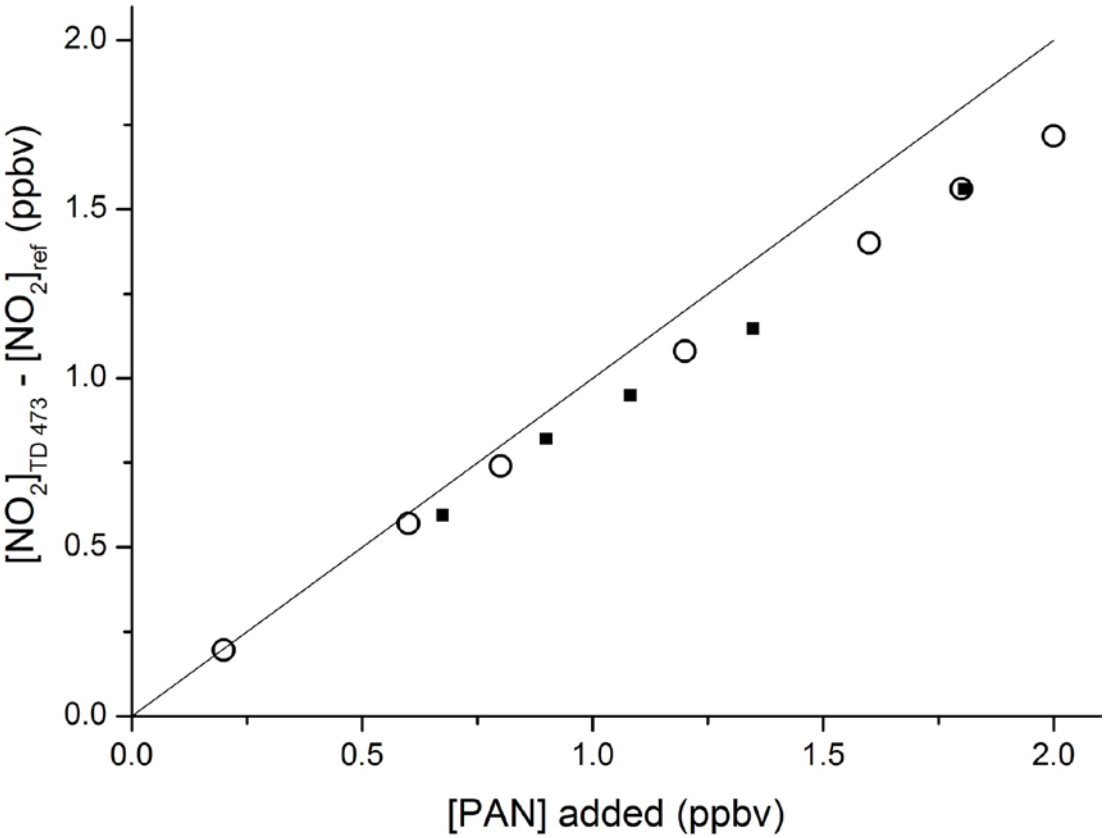

Figure S7 Measurement (solid squares) and modelling (open circles) of PAN generated in the photochemical PAN source. PAN added is calculated assuming 95 % conversion of NO. The open circles are the model prediction. The straight line represents 1:1 conversion of PAN to NO_2. The observed deviation from the straight is reproduced by the model, and confirming the results of the experiments in which NO and NO_2 were added.

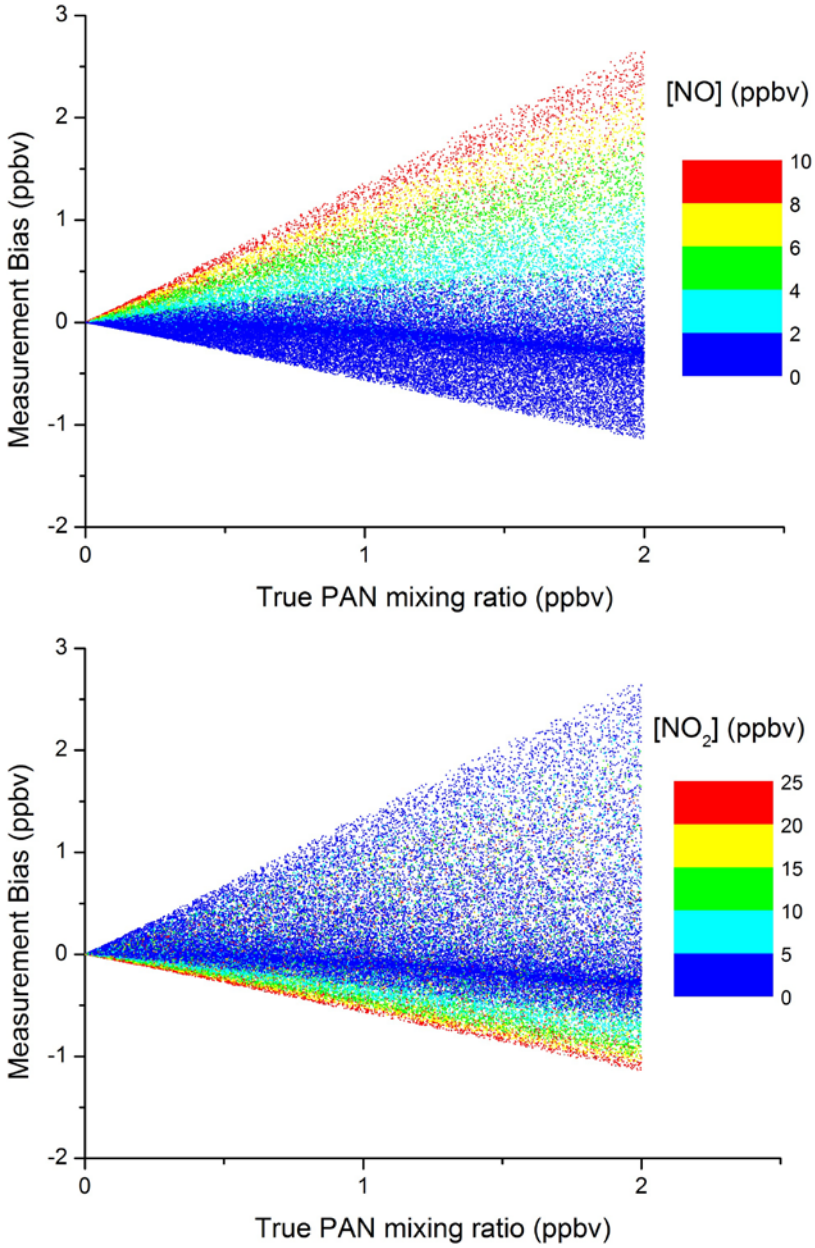

Figure S8. Result of ~90000 simulations of the inlet / cavity chemistry initiated with various NO, NO_2 and PAN concentrations, the range of which was selected to cover the values observed at the PARADE field campaign. A large measurement positive bias is associated with high NO or low NO_2 and vice-versa.

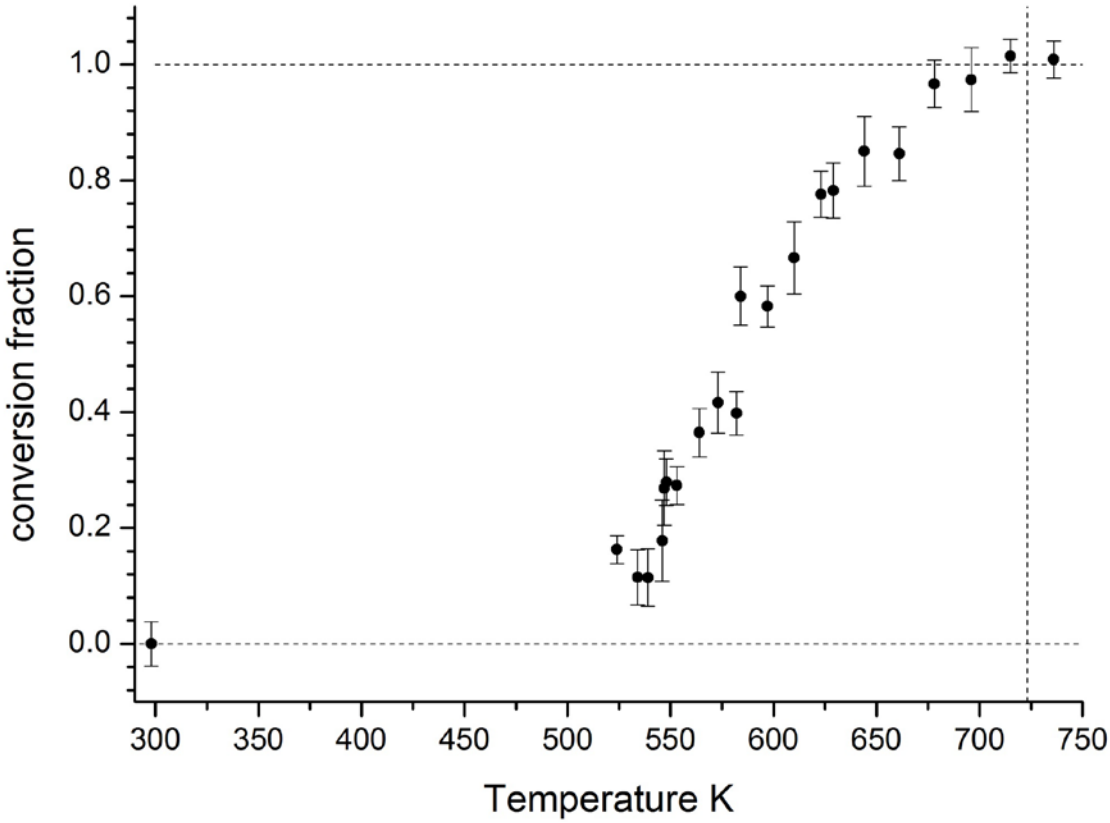

Figure S9. Thermal decomposition of $ClNO_2$ in the 723 K inlet. The horizontal, dashed lines indicate the 0 and 100 % conversion efficiencies. The vertical dashed lines indicates the temeprature at which the inlet was operated (723 K) when measuring ΣANs.

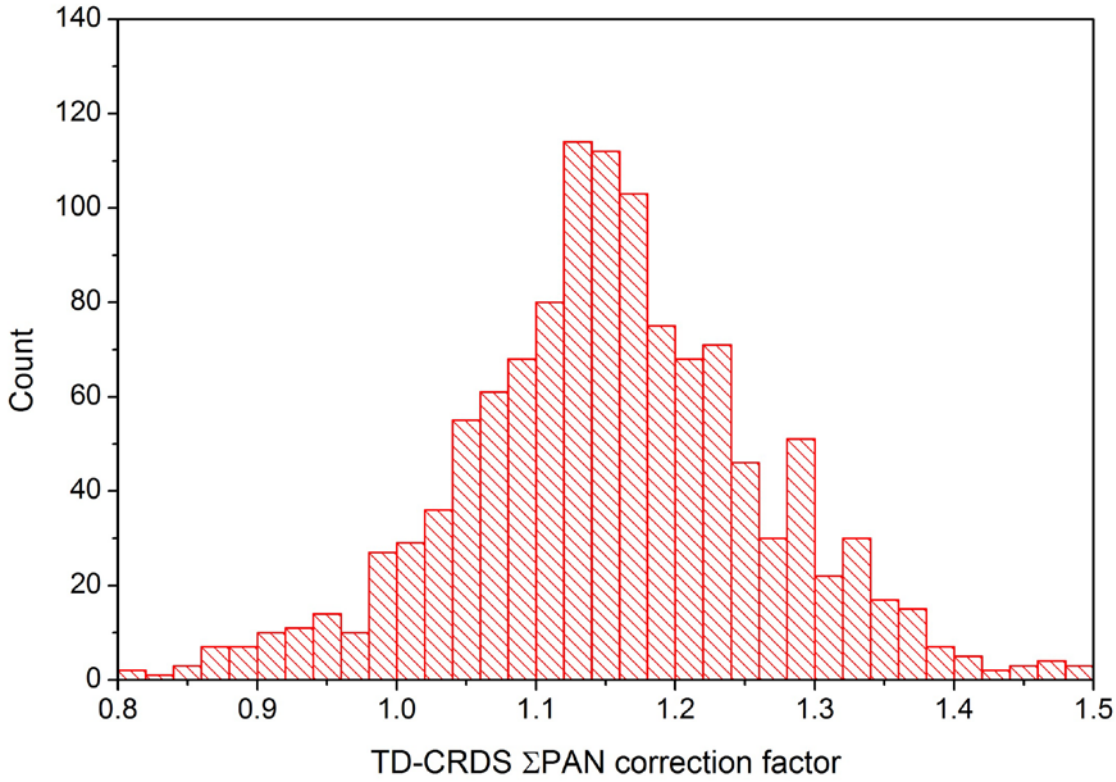

Figure S10. Frequency distribution of the simulation derived correction factors for the TD-CRDS measurements of ΣPNs during the PARADE campaign.

Chemical scheme used in the numerical simulations.

```
k1                  : PAN = CH3CO3 + NO2
k2                  : CH3CO3 + NO2 = PAN
k3                  : CH3CO3 + NO = CH3CO2 + NO2
k3a                 : CH3CO2 = CH3O2 + CO2
k4                  : CH3O2 + NO = HCHO + HO2 + NO2
k5                  : CH3O2 + NO2 = CH3O2NO2
k6                  : CH3O2NO2 = CH3O2 + NO2
k7                  : HO2 + NO = NO2 + OH
k8                  : HO2 + NO2 = HO2NO2
k9                  : HO2NO2 = HO2 + NO2
k10                 : OH + NO2 = HNO3
k11                 : OH + NO = HONO
k12                 : CH3CO3 + CH3CO3 = CH3CO2 + CH3CO2
k13                 : CH3CO3 + CH3O2 = HCHO + HO2 + CH3O2 + co2
k14*0.29            : CH3CO3 + HO2 = PAA + O2
k14*0.1             : CH3CO3 + HO2 = AA + O3
k14*0.61            : CH3CO3 + HO2 = OH + CH3O2
k15                 : CH3O2 + HO2 = CH3OOH
k16                 : HO2 + HO2 = H2O2
k17                 : OH + HO2 = h2o + o2
k18                 : IPN = IPO + NO2
k19                 : IPO + O2 = HO2 + acetone
k19a                : IPO + O2 = CH3O2 + CH3CHO
k26                 : OH + CH3CHO = CH3CO
k20                 : CH3CO3 = CH3CO
k21                 : CH3CO3 = CH2COOOH
k23                 : CH2COOOH = CH2CO2 + OH
k24                 : CH3CO + O2 = CH3CO3
k24a                : CH3CO + O2 = OH + CH2CO2
k25                 : CH3CO = CH3O2
k26                 : OH + CH3O2 = HO2 + HO2
k27                 : OH + CH3CO3 = HO2 + CH3O2 + CO2

Note that the reactions are not numbered the same as in the manuscript
IPN = 2-propyl nitrate
IPO = C3H7O


k1 = ((1.10e-5*exp(-10100/T))*M*
(1.9e17*exp(-14100/T)))/((1.10e-5*exp(-10100/T))*M+
(1.9e17*exp(-14100/T)))*10^(log10(0.3)/
(1+(log10((1.10e-5*exp(-10100/T))*M/
(1.9e17*exp(-14100/T)))/(0.75-1.27*log10(0.3)))^2))

k2 = ((3.28e-28*(T/300)^-6.87)*M*
(1.125e-11*(T/300)^-1.105))/((3.28e-28*(T/300)^-6.87)*M+
(1.125e-11*(T/300)^-1.105))*10^(log10(0.3)/
(1+(log10((3.28e-28*(T/300)^-6.87)*M/
(1.125e-11*(T/300)^-1.105))/(0.75-1.27*log10(0.3)))^2))

k3 = 7.5e-12*exp(290/T)

k3a = 1e6
```

```
k4 = 2.3e-12*exp(360/T)

k5 = ((2.5e-30*(T/300)^-5.5)*M*
(1.8e-11))/((2.5e-30*(T/300)^-5.5)*M+
(1.8e-11))*10^(log10(0.36)/(1+(log10((2.5e-30*(T/300)^-5.5)
*M/(1.8e-11))/(0.75-1.27*log10(0.36)))^2))

k6 = ((9e-5*exp(-9690/T))*M*
(1.1e16*exp(-10560/T)))/((9e-5*exp(-9690/T))*M+
(1.1e16*exp(-10560/T)))*10^(log10(0.36)/
(1+(log10((9e-5*exp(-9690/T))*M/
(1.1e16*exp(-10560/T)))/(0.75-1.27*log10(0.36)))^2))

k7 = 3.45e-12*exp(270/T)

k8 = ((1.4e-31*(T/300)^-3.1)*M*
(4.0e-12))/((1.4e-31*(T/300)^-3.1)*M+
(4.0e-12))*10^(log10(0.4)/(1+(log10((1.4e-31*(T/300)^-3.1)
*M/(4.0e-12))/(0.75-1.27*log10(0.4)))^2))

k9 = (4.1e-5*exp(-10650/T))*M*
(6.0e15*exp(-11170/T)))/((4.1e-5*exp(-10650/T))*M+
(6.0e15*exp(-11170/T)))*10^(log10(0.4)/
(1+(log10((4.1e-5*exp(-10650/T))*M/
(6.0e15*exp(-11170/T)))/(0.75-1.27*log10(0.4)))^2))

k10 = ((3.2e-30*(T/300)^-4.5)*M*
(3.0e-11))/((3.2e-30*(T/300)^-4.5)*M+
(3.0e-11))*10^(log10(0.41)/(1+(log10((3.2e-30*(T/300)^-4.5)
*M/(3.0e-11))/(0.75-1.27*log10(0.41)))^2))

k11 = ((7.4e-31*(T/300)^-2.4)*M*
(3.3e-11*(T/300)^-0.3))/((7.4e-31*(T/300)^-2.4)*M+
(3.3e-11*(T/300)^-0.3))*10^(log10(0.81)/
(1+(log10((7.4e-31*(T/300)^-2.4)*M/
(3.3e-11*(T/300)^-0.3))/(0.75-1.27*log10(0.81)))^2))

k12 = 2.9e-12*exp(500/T)

k13 = 2.0e-12*exp(500/T)

k14 = 7.6e-13*exp(980/T)

k15 = 3.8e-13*exp(780/T)

k16 = (2.2e-13*exp(600/T) + 1.9e-33*M*exp(980/T))

k17 = 4.8e-11*exp(250/T)

k18 = 3.16e16*exp(-20129/T)

k19 = 1.9e-14*exp(-300/T)

k19a = 5.33e19*T^-1.7*exp(-8630/T)

k20 = 1.5e16*exp(-20000/T)
```

```
k21 = (0.20) * 1.6e16*exp(-20000/T)

k23 = 1.8e18*exp(-20000/T)

k24 = (HPL24*LPL24*M/(LPL24*M+HPL24))*
0.8^((1+(log10(LPL24*M/HPL24))^2)^-1)
LPL24 = 7.39e-30*(T/300)^-2.2
HPL24 = 4.88e-12*(T/300)^-0.85

k24a = kint*(1-k24/HPL24)
kint = 6.4e-14*exp(820/T)


k25 =((1.0e-8*exp(-7080/T))*M*
(2.0e13*exp(-8630/T)))/((1.0e-8*exp(-7080/T))*M+
(2.0e13*exp(-8630/T)))*10^(log10(0.5)/(1+(log10(
(1.0e-8 *exp(-7080/T))*M/(2.0e13*exp(-8630/T)))/
(0.75-1.27*log10(0.5)))^2))

k26 = k27 = 2e-10
```

Rate coefficients were taken from IUPAC where available: (IUPAC, 2015)

Exceptions are:

k3a	Chosen to be essentially instantaneous
k14	Rate coefficient and branching ratio for OH formation from (Groß et al., 2014)
k18	2-propyl nitrate thermal decomposition rate constant from (Day et al., 2002)
k20-24	See text in manuscript.
k25	(Baulch et al., 2005)
k26, k27	~collision rate (Bossolasco et al., 2014;Farago et al., 2015)

References

Baulch, D. L., Bowman, C. T., Cobos, C. J., Cox, R. A., Just, T., Kerr, J. A., Pilling, M. J., Stocker, D., Troe, J., Tsang, W., Walker, R. W., and Warnatz, J.: Evaluated kinetic data for combustion modeling: Supplement II, J. Phys. Chem. Ref. Data, 34, 757-1397, 2005.

Bossolasco, A., Farago, E. P., Schoemaecker, C., and Fittschen, C.: Rate constant of the reaction between CH_3O_2 and OH radicals, Chem. Phys. Lett., 593, 7-13, 10.1016/j.cplett.2013.12.052, 2014.

Day, D. A., Wooldridge, P. J., Dillon, M. B., Thornton, J. A., and Cohen, R. C.: A thermal dissociation laser-induced fluorescence instrument for in situ detection of NO_2, peroxy nitrates, alkyl nitrates, and HNO_3, J. Geophys. Res., 107, 4046-, 2002.

Farago, E. P., Schoemaecker, C., Viskolcz, B., and Fittschen, C.: Experimental determination of the rate constant of the reaction between $C_2H_5O_2$ and OH radicals, Chem. Phys. Lett., 619, 196-200, 10.1016/j.cplett.2014.11.069, 2015.

Groß, C. B. M., Dillon, T. J., Schuster, G., Lelieveld, J., and Crowley, J. N.: Direct kinetic study of OH and O_3 formation in the reaction of $CH_3C(O)O_2$ with HO_2, The Journal of Physical Chemistry A, 118, 974-985, doi:10.1021/jp412380z, 2014.

IUPAC: Task Group on Atmospheric Chemical Kinetic Data Evaluation, (Ammann, M., Cox, R.A., Crowley, J.N., Jenkin, M.E., Mellouki, A., Rossi, M. J., Troe, J. and Wallington, T. J.) http://iupac.pole-ether.fr/index.html., 2015.